Embedded System for Distance Measurement and Surface Discrimination Applications

Hélène Tap, Laurent Gatet, Emmanuel R. Moutaye, Blaise Mulliez

Embedded System for Distance Measurement and Surface Discrimination Applications

Hélène Tap, Laurent Gatet, Emmanuel Moutaye, Blaise Mulliez
Université de Toulouse, LAAS-CNRS, CNRS, INP-ENSEEIHT
2 Rue C. Camichel, BP 7122, 31071 Toulouse Cedex 7, France
helene.tap@enseeiht.fr

***Abstract*—The development of robotics and miniaturization has lead to the design of intelligent embedded sensors capable of measuring distance either on wide ranges or with high resolution. Yet, it is impossible to gather both information at the same time performing a single measurement. Furthermore, the enlightened surface type may be detected only under well-known experimental conditions. Computer processing is also often necessary to analyze the sensors data.**

In this paper, we report an embedded sensor capable of measuring distances with a resolution of 250 μm in a range of 2.7 m and of discriminating a wide variety of surface types. The embedded system is based on a phase-shift laser rangefinder, whose essential components are a Laser Diode (ML4412N) and its intelligent CMOS laser driver circuit, a CMOS Avalanche PhotoDiode (APD) and its transimpedance circuit and a CMOS Analog Neural Network.

I. Introduction

Embedded systems for distance measurement and obstacles detection are now essential in various fields like robotics [1], transportation [2], medical applications [3] and security systems [4]. Among the various existing time-of-flight distance determination techniques [5], the phase-shift measurement is one of the most appropriate to achieve a high-resolution on the widest possible range [6]. Nevertheless, the design of an optimized intelligent embedded system based on this method leads to several issues.

First, the light emitted by the Laser Diode (LD) is modulated at a high frequency f_{RF}, reflected by a non-cooperative target and subsequently detected by a photodiode. The phase-shift $\Delta\phi$ measured between the photoelectric signal and the light modulation signal is directly proportional to the round-tripe time-of-flight and consequently to the distance D between the system and the target. The first problem is linked to the variations of the LD threshold current I_{th}, whose value can strongly vary with the temperature and from one LD to another. However, in order to maximize the optical power modulation, the LD has to be used in its whole linearity domain. Thus, an intelligent laser driver circuit must be built to optimize the dynamics of any LD and to avoid its destruction in extreme temperature conditions.

Then, the phase-shift measurement may be made easier through a heterodyne technique [7]. For this matter, one solution uses an electrical mixing. In this case however, the transimpedance amplifier operates at high frequency f_{RF} that creates a large noise spectral density of the photoelectric signal. A second technique uses an optoelectronic mixing through an Avalanche PhotoDiode (APD). The transimpedance amplifier operates then at a low frequency that decreases the noise spectral density. Nevertheless, the high supply voltage usually needed to bias the APD (300-400 V) is not compatible with an embedded system. Ultimately, the second challenge is the design of an APD operating at low voltage and in a technology compatible with its following transimpedance circuit.

Eventually, since the phase-shift measurement $\Delta\phi$ is performed modulo 2π, the maximum measurement range without indecision Λ, inversely proportionally to f_{RF}, is limited. However, since the device sensitivity is proportional to f_{RF}, it is not possible to achieve a high-resolution measurement on a wide range. To alleviate this limitation, one solution consists in using two modulation frequencies of the LD [8]. Yet, one major drawback of this solution is to make the system far more complicated. A second solution is to implement a Neural Network (NN) used as a linearizer in the laser rangefinder photoreception head [9]. Not only does this solution not make the system more complicated, but also NN may be used to implement new functions, like surface discrimination [10]. Consequentely, the third issue is the development of a high-resolution embedded system based on a NN and capable of working in a large distance range .

This paper presents an intelligent embedded system developed in order to respond to the three aforementioned problems. The developed embedded system, dedicated to distance measurement, is based on a phase-shift laser rangefinder using optoelectronic mixing through an APD (Fig. 1). The components have been specifically designed and optimized to respond to the three challenges and to be integrated in an embedded system. CMOS technologies have been chosen for low bulk, low consumption and low cost reasons [11]. The components are detailed in the following parts.

II. CMOS laser driver circuit

When designing a CW semiconductor laser-based devices, the laser source life span is a prominent problem. Telecommunications laser drivers can accurately control the average emitted optical power [12], [13], but their transient response is generally not thoroughly studied. Nevertheless, when the power supply is quickly switched on or off, the feedback loop may impose a strong bias current that makes the laser exceed

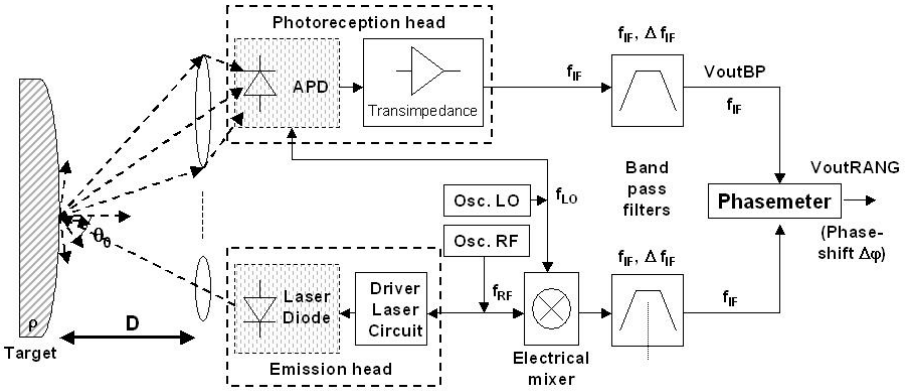

Fig. 1. Block diagram of the laser rangefinder. The non-linear property of the current-voltage characteristic of the APD, biased in the avalanche zone, is used in order to mix the photoelectric current at f_{RF} with the Local Oscillator (LO) signal. The phase-shift $\Delta\phi$ is measured at an Intermediate Frequency $f_{IF} \approx 1$ kHz using optoelectronic mixing that preserves the phase-shift against the distance.

its maximal optical power. In such a case, the LD crystal mirror suffers from catastrophic damage and the effect on its reflectivity only may produce a drastic laser optical output deterioration [14].

With a closed-loop laser driver, the average output power is forced by comparison with a reference voltage [15]. LD threshold current dispersion and temperature effects are then taken into account. Nevertheless, the study of the frequency response and the feedback stability are fundamental.

An optical feedback laser driver circuit has been developed in 0.6 μm CMOS technology to control the average optical output power of a double heterostructure CW LD but also to operate with a wideband amplitude modulation (Fig 2.a). Safety features, including transient signal suppression, protect the laser from excessive light power.

The average light power monitoring is realized by measuring the photoelectric current of a PIN photodiode integrated inside the package of the LD. The photodiode delivers an average photoelectric current $< I_{ph} >$ proportional to the average optical power $< P_{LD} >$, for bias current $I_{LD} > I_{th}$ where:

$$< I_{ph} >= \alpha S_\lambda < P_{LD} > \equiv a_{ph}(< I_{LD} > -I_{th}) \quad (1)$$

with α a proportionality coefficient, S_λ the photodiode spectral response (A/W) and a_{ph} the optical feedback factor.

The modulation current $\Delta I(t)$ is given by a differential circuit based on an emitter-coupled pair. This differential stage is biased by a constant current source I_{ref} such as:

$$I_{ref} = \Delta I_{pp,max} \quad (2)$$

with $\Delta I_{pp,max}$ the maximal amplitude of the AC bias current (Fig 2.b). Without the modulation alternative signal ($\Delta I(t) = 0$), the laser diode current is supplied by the differential amplifier. A DC current source supplies the minimum threshold current $I_{th,min}$ in the temperature range. The optical power is controlled by an additional feedback current $I_{cont} = I_{th} - I_{th,min}$. Its maximal value is equal to $I_{th,max} I_{th,min}$. Therefore, the LD bias current is given by:

$$I_{LD}(t) = I_{cont} + I_{th,min} + I_{mod} \quad (3)$$

with I_{mod} the current issued from the differential pair:

$$I_{mod} = I_{ref}/2 + \Delta I(t) \quad (4)$$

The feedback loop stability has been studied. Two transconductance structures using inverting and non-inverting circuits have been compared using the dominant pole compensation method [16]. Calculations, suported by simulations, have shown that the inverting structure is the most stable. The closed loop frequency response of the inverting laser driver has then been evaluated for different values of the capacitor C_1 (Fig 2.c). This circuit is implemented in the emission optical head of the distance measurement embedded system, in order to drive the ML4412N LD (characteristics in Tab. I).

TABLE I
ML4412N LASER DIODE PARAMETERS, WITH $< P_{LD} >$ = 3MW

$I_{th,min}$	I_{th}	$I_{th,max}$	η	a_{ph}
25 mA	30 mA	40 mA	0.3 mW/mA	$3.2{\cdot}10^{-2}$

I_{th}, $I_{th,min}$ and $I_{th,max}$ are respectively the typical, the minimum and the maximum threshold current values. η is the differential efficiency and a_{ph} is the transfer factor between laser diode bias current and photodiode current.

III. CMOS AVALANCHE PHOTODIODE (APD)

The Avalanche PhotoDiode (APD) is the keystone of the accurate embedded system for distance measurement.

The integration of an APD in a CMOS technology requires that a sufficient voltage, allowing avalanche mode of the vertical junction without breaking out the peripheral junction, may be applied. For that matter, the device must be protected against excessive horizontal electric fields. A solution is to implement a guard ring around the photodiode to prevent any damage to the device [17].

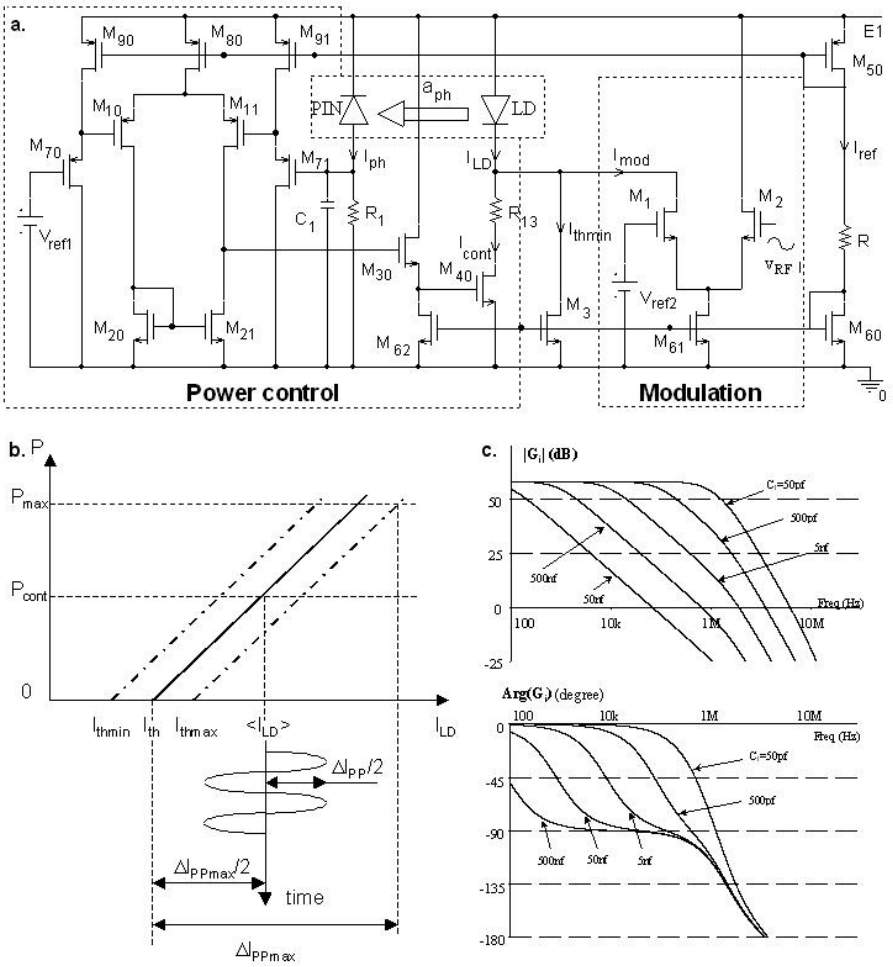

Fig. 2. Laser driver circuit
a. CMOS laser driver circuit based on an optical feedback. A PIN photodiode is integrated in the LD case. $I_{th,min}$, provided by a DC current source, is the minimum threshold current in a given temperature range. I_{mod} is the current issued from a differential circuit based on an emitter-coupled pair. I_{cont} is an additional feedback current imposed by the optical power received by the PIN photodiode.
b. Laser Diode light power versus bias current. $\Delta I_{pp,max}$ represents the maximal amplitude of the AC bias current.
c. Magnitude $\mid G_i \mid_{dB}$ and phase-shift Arg(G_i) frequency responses of the laser driver circuit current loop gain for different values of C_1 (Laser Diode ML4412, $R_1 = 3750\Omega$).

Another drawback to tackle with is the semiconductor absorption coefficient that depends on the light wavelength. CMOS APDs show a better response for short wavelengths because the photons absorption depth in silicon at 400 nm is 0.4 μm [19]. This value is equivalent to the junction depth (0.2 μm in 0.35 μm CMOS technology) plus the depletion layer width when the junction is reverse-biased. Since the multiplication of the photogenerated carriers is made in the depletion layer - that is to say in the region where electric field is maximal -, multiplication and absorption zones are nearly merged. As a consequence, APDs integrated in CMOS technology exhibit poorer performances than the bulky ones.

Nevertheless, CMOS APDs show undeniable advantages. First, they have an interesting internal gain. Then, the possibility to integrate the transimpedance circuit on the same silicon bulk allows reducing efficiently parasitic capacitors. Finally, the low supply voltage needed to be in avalanche mode is a strong advantage for an embedded distance measurement system.

A short-wavelength P+N APD has been implemented in a commercial 0.35 μm CMOS technology (Fig. 3.a). The anode is formed by a P+ diffusion originally expected for implementing the source or the drain of a PMOS transistor. The cathode is made with a N-well originally expected for implementing the bulk of a PMOS transistor. The active region surface is $3.78{\cdot}10^{-3}$ cm^2. An efficient guard-ring structure has been created using the lateral diffusion of two N-well regions separated by a gap of 1.2 μm. When the CMOS APD is biased at 2 V, the best responsiveness $S_{\lambda,APD} = 0.11A/W$ is obtained at $\lambda = 500$ nm. This value could easily be improved by using an anti-reflection coating. At $\lambda = 472$ nm, the internal gain is about 75 at 6 V and 157 at 7 V (Fig. 3.b). When biased at 6 V, the APD has a dark current of 128 μA.mm^{-2} and an excess noise factor $F = 20$ [18]. These performances

make the device usable as a satisfying optoelectronic mixer in the low power integrated optical head of the phase-shift laser rangefinder (Fig. 3.c).

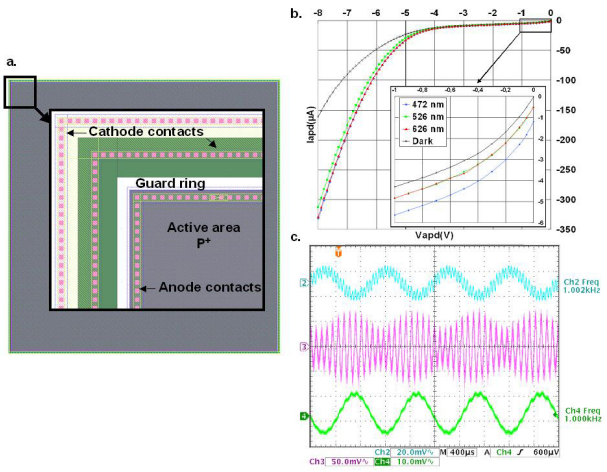

Fig. 3. CMOS Avalanche Photodiode.
a. Layout of the APD in 0.35 μm CMOS technology. The N-well is split into two N-tubs separated by a small interval (1.2 μm) forming the guard ring. The active area is 615 μm x 615 μm.
b. Reverse-biased characteristic I(V) of the CMOS APD for different lighting conditions. The Laser Diodes references are: HLMP-EG32-NR000 (626 nm); HLMP-CM30-M0000 (526 nm); HLMP-CB31-M0000 (472 nm).
c. Channel 2: reference mixing at the electronic mixer output; Channel 3: optoelectronic mixing at the transimpedance circuit output; Channel 4: optoelectronic mixing after the band-pass filter. The Intermediate Frequency f_{IF} (1 kHz) is equivalent to the difference between the Reference Frequency f_{RF} (1.001 MHz) and the Local Oscillator frequency f_{LO} (1 MHz). The APD is biased at -6 V and $\lambda = 472$ nm.

IV. CMOS Neural Network

The phase-shift measurement method allows a high-resolution on the widest possible range. The phase-shift $\Delta\phi$ between the photoelectric current and the light modulation signal (Fig. 1) is given by:

$$\Delta\phi = 2\pi f_{RF}\tau_D \tag{5}$$

where $\tau_D = 2D/c$ is the round-trip time-of-flight and c the light velocity.

The rangefinder output signal $V_{out,RANG}$ is proportional to the phase-shift and then to the distance D:

$$V_{out,RANG} = K \cdot \Delta\phi = K_2 D \tag{6}$$

with K the proportionality coefficient between the phase-shift and the rangefinder output signal and K_2 the proportionality coefficient between the distance and the rangefinder output signal.

The device sensitivity response S_D is:

$$S_D = \frac{\delta D}{\delta\phi} = \frac{c}{4\pi f_{RF}} \tag{7}$$

The maximum measurement range Λ without indecision is then:

$$\Lambda = \frac{c}{2f_{RF}} \tag{8}$$

To optimize the resolution ($S_D = 2.5$mm /degree), a high frequency value is required (f_{RF} = 166MHz), which leads to a small measurement range ($\Lambda = 90$ cm). To easily perform the distance measurement, the measurement frequency f_{IF} is decreased to 1 kHz by optoelectronic heterodyning through the CMOS APD (Fig. 1).

To increase Λ without decreasing S_D, the idea is to extract the information on distance D contained in the filtered photoelectric signal amplitude $V_{out,BP}$, measured at the band pass filter output (Fig. 1):

$$V_{out,RANG} = K_1 \frac{\rho \cdot cos(\theta_0)}{D^2} \tag{9}$$

with K_1 a constant, ρ the non-cooperative target diffusing reflection coefficient, characteristic of the surface tested type [20] and θ_0 the incidence angle.

By measuring $V_{out,BP}$ and by linearising this formula, the distance D can be evaluated without indecision but with a low resolution. Thus, thanks to the phasemeter measurement $V_{out,RANG}$, a high resolution may be obtained on a wide distance range.

Furthermore, knowing the distance D, different targets types may be discriminated by extracting the coefficient ρ from $V_{out,BP}$.

Using a Neural Network (NN), it is possible to correct non-linearities and to perform surface classification, depending on the sensor environment [21], [22]. That is why a generic NN has been developed to achieve both tasks. In the first case, the NN is used as a linearizer [9]. A precision of $\Lambda/2$ on the distance D is sufficient to avoid any ambiguity. In the second case, the NN is used as a classifier [10]. In order to perform surface discrimination in a wide range, the NN requires two inputs: $V_{out,BP}$ and $V_{out,RANG}$.

The generic analog NN, composed of two inputs, one output and a single hidden layer with three processing neurons (Fig. 4.a), has been implemented in 0.35 μm CMOS technology (Fig. 4.b) [23]. It approximates the distance with a satisfaying precision in a range three times wider than the one limited by the $2k\pi$ indecision. (Fig. 4.c). Moreover, it is capable of discriminating four types of surfaces (plastic surface, glossy paper, painted wall and porous surface) for distances D and incidence angles θ_0 varying between [0.5 m ; 1.25 m] and [$-\pi$/6;π/6] respectively. An example of surface recognition is shown in Fig. 4.d for a glossy paper (surface S_2).

The NN average current consumption is equal to 15 mA. Since the whole system is analog, detection time is only limited by the bandwidth of each analog part of the system that is higher than 1 MHz. Thus, surface detection is achieved in less than 1 μs.

V. Discussion

An embedded system based on a phase-shift laser rangefinder has been developed for distance measurement.

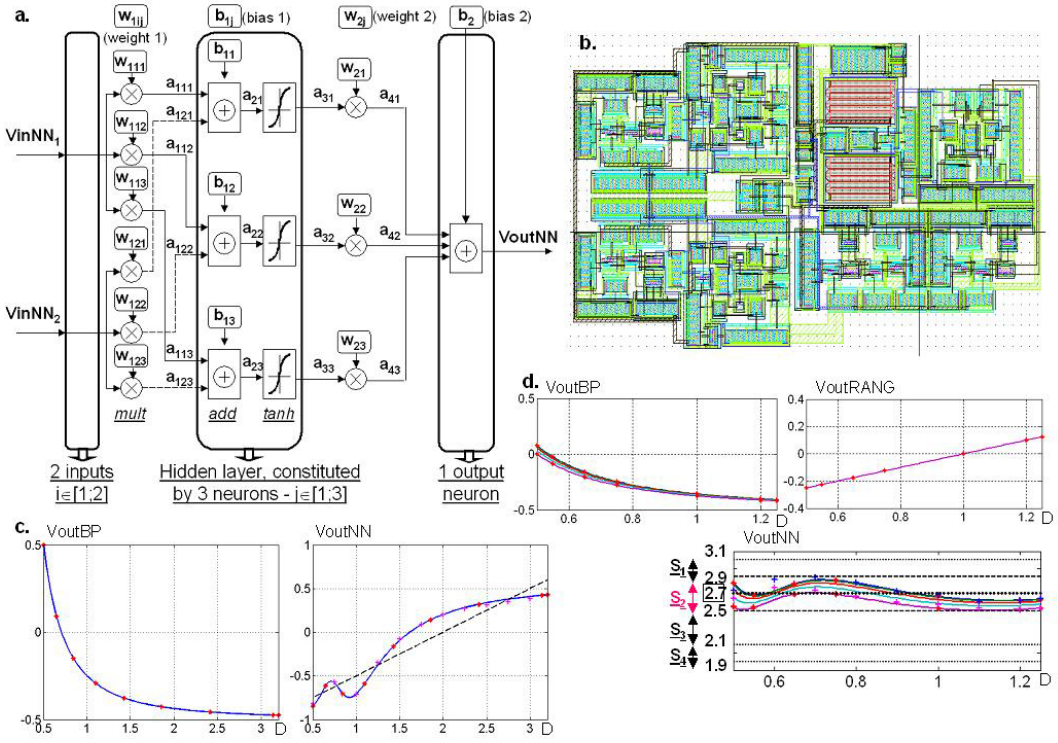

Fig. 4. CMOS Neural Network
a. Neural network architecture. It is composed by two inputs (V_{in,NN_1} and V_{in,NN_2}, respectively linked to $V_{out,BP}$ and $V_{out,RANG}$), one output neuron ($V_{out,NN}$) and a single hidden layer with three processing neurons, which activation function is a sigmoid (tanh).
b. Neuron layout in 0.35 μm CMOS technology. Size: 276 μm x 148 μm.
c. On the left: first NN input (the second one is linked to ground). On the right: NN output. The dashed line, the solid curve and crosses represent ideal output, simulation and experimental points respectively.
d. On the top left: first NN input $V_{out,BP}$ corresponding to the surface S_2 for various incidence angles θ_0. On the top right: second NN input $V_{out,RANG}$. On the bottom: NN output. The dashed line, the solid curve and crosses represent ideal output, simulation and experimental points respectively. The NN output remains in the voltage interval [2.5 V ; 2.9 V] dedicated to surface S_2.

Regarding the emission optical head, a CMOS analog intelligent laser driver circuit has been designed and tested. It is unconditionally stable and self-adapted to different LD current-power characteristics and to temperature variations. In order to protect the LD against over-currents caused by the switch-on of the supply voltage, a "slow start switch on" circuit could be added.

The photoreception optical head has been developed to be compatible with embedded systems. Measurement resolution and signal to noise ratio have been improved by integrating an optoelectronic heterodyning system instead of an electrical one. Previously, the design of a 0.6 μm CMOS dual photosensor [24] has to be aborted because of a too low cut-off frequency for laser range-finding applications. Then, a low-voltage CMOS APD has been designed to allow high-precision and high-SNR in the embedded measurement system. The implementation of an array of APDs in CMOS technology with a preamplifier circuit close to each photodetector may still improve the bandwidth and signal-to-noise ratio performances of the device [25].

Finally, the analog implementation of a generic CMOS NN enables two additional tasks: increasing three times the measurement range without lowering resolution and discriminating different surfaces types. Besides, a NN digital integration in a FPGA has led to the comparison between both types of implementation [26].

In order to accurately measure the phase-shift, analog and digital phasemeters have also been proposed with a resolution of 0.1° [27]. Through the distance measurement embedded system, a sensitivity of 250 μm may be reached.

These different electronic or optical functions, detailled in previous publications, have been specifically developed and optimized for the whole embedded distance measurement system presented in this paper. These encouraging overall results foresee the impending development of a 3D-camera System-On-Chip (SOC) (Fig. 5) with high-accuracy, high SNR, high distance range and low supply voltage. For robotics applications, the scanning system must be of small size and as fast as possible. One solution is to deflect the laser beam with two micro-mirrors. A 3D-camera using a PIN photodiode has already been developed in the range [0.5 m ; 10 m] with a resolution of 1.4 cm [28]. Its performances are quite poor in terms of accuracy and SNR because a PIN photodiode has been used and a large distance range has been favored. Furthermore, its realization based on Printed Circuit Boards (PCB) leads to an important global size (1.2 dm^3) and high

power consumption.

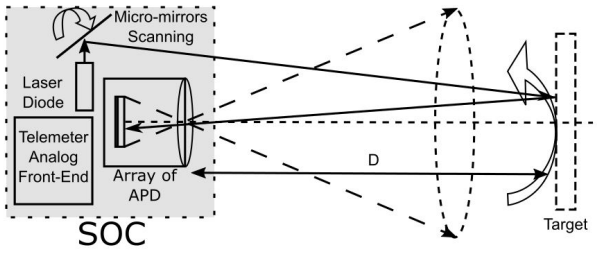

Fig. 5. Block diagram of Distance measurement System-On-Chip (SOC) using an APDs array and micro-mirrors.

The use of integrated functions such as CMOS laser driver circuit, CMOS APD and CMOS analog NN will considerably improve the performances and the power consumption of the 3D-camera SOC.

REFERENCES

[1] Hussein, A., Marìn-Plaza, P., Martìn, D., De La Escalera, A., Armingol, J. M.: 'Autonomous off-road navigation using stereo-vision and laser-rangefinder fusion for outdoor obstacles detection', *2016 IEEE Intelligent Vehicles Symposium (IV)*, 2016, pp. 104-109

[2] Mancini, A., Frontoni, E., Zingaretti, P.: 'Embedded Multisensor System for Safe Point-to-Point Navigation of Impaired Users', *IEEE T. Intell. Transp. Syst.*, 2015, **16(6)**, pp. 3543-3555

[3] Parikh, S.P., Grassi Jr., V., Kumar, V., Okamoto Jr., J.: 'Integrating Human Inputs with Autonomous Behaviors on an Intelligent Wheelchair Platform', *Intell. Syst.*, 2007, **22(2)**, pp. 3341

[4] Buttgen, B., Lustenberger, F., Seitz, P.: 'Demodulation Pixel Based on Static Drift Fields', *IEEE T. Electron. Dev.*, 2006, **53(11)**, pp. 27412747

[5] Bosch, T., Lescure, M.: 'Selected Papers on Laser Distance Measurement'. (*SPIE Milestone Serie, volume MS115*, USA, 1995)

[6] Amann, M.C., Bosch, T., Lescure, M., Myllyl, R., Rioux, M.: 'Laser Ranging: a Critical Review of Usual Techniques for Distance Measurement', *Opt. Eng.*, 2001, **40(1)**, pp. 10-19

[7] Dupuy, D., Lescure, M., Tap-Béteille, H.: 'Analysis of an Avalanche Photodiode used as an Optoelectronic Mixer for a Frequency Modulated Continuous Wave Laser Range Finder', *J. Opt. A: Pure Appl.Opt.*, 2002, **4**, pp. 332-336

[8] Poujouly, S., Journet, B.: 'A Twofold Modulation Frequency Laser Range Finder', *J. Opt. A: Pure Appl. Opt.*, 2002, **4**, pp. S356-S363

[9] Gatet, L., Tap-Béteille, H., Lescure, M.: 'Measurement Range Increase of a Phase-Shift Laser Rangefinder using a CMOS Analog Neural Network', *IEEE T. Instrum. Meas.*, 2009, **58(6)**, pp. 1911-1918

[10] Gatet, L., Tap-Béteille, H., Lescure, M.: 'Real Time Surface Discrimination using an Analog Neural Network implemented in a Phase-Shift Laser Rangefinder', *IEEE Sens. J.*, 2007, **7(10)**, pp. 1381-1387

[11] Qu, H., Xie, H.: 'Process Development for CMOS-MEMS Sensors With Robust Electrically Isolated Bulk Silicon Microstructures', *J. Microelectromech. S.*, 2007, **16(5)**, pp. 11521161

[12] Chen, L.P., Li, M.Y., Chang-Hasnain, C.J., Lau, K.Y.: 'A Low-Power 1-GB/s CMOS Laser Driver for a Zero-Bias Modulated Optical Transmitter', *IEEE Photonic. Tech. L.*, 1997, **9(7)**, pp. 997-999

[13] Thompson, M.T., Schlecht, M.F.: 'High Power Laser Diode Driver Based on Power Converter Technology', *IEEE T. Power Electr.*, 1997, **12(1)**, pp. 46-52

[14] Eliseev, P.G.: 'Degradation of injection laser', *IEEE J. Lumin.*, 1973, **7**, pp. 338-356

[15] Sckinger, E., Ota, Y., Gabara, T., Fisher, W.: 'A 15 mW, 155 Mb/s CMOS Burst-Mode Laser Driver with Automatic Power Control and End-of-Life Detection', *IEEE J. Solid-St. Circ.*, 1999, **34(12)**, pp. 1944-1950

[16] Zivojinovic, P., Lescure, M., Tap-Béteille, H.: 'Design and Stability Analysis of a CMOS Feedback Laser Driver', *IEEE T. Instrum. Meas.*, 2004, pp. 102-108

[17] Rochas, A. et al.: 'Low-Noise Silicon Avalanche Photodiodes Fabricated in Conventional CMOS Technologies', *IEEE T. Electron Dev.*, 2002, **49(3)**, pp. 387-394

[18] Moutaye, E., Tap-Béteille, H.: 'CMOS Avalanche Photodiode Embedded in a Phase-Shift Laser Rangefinder', *IEEE T. Electron Dev.*, 2008, **55(12)**, pp. 3396-3401

[19] Sze, S. M.: 'Physics of Semiconductor Devices', (*J. Wiley*, New York, 1981)

[20] Bosch, T., Lescure, M.: 'Experimental Determination of the Useful Reflexion Coefficient of Non-Cooperative Targets for a Time-of-Flight Laser Rangefinder', *Opt. Rev.*, 1995, **2(4)**, pp. 289-291

[21] Ozdemir S.K., Shinohara S., Ito S., Takamiya S., Yoshida H.: 'Compact Optical Instrument for Surface Classification using Self-Mixing Interference in a Laser Diode', *Opt. Eng.*, 2001, **40(1)**, pp. 38-43

[22] Neelamegan P., Rajendran A.: 'Classification of Surface Roughness and Distance Measurement using Artificial Neural Network', *Instrum. Sci. Technol.*, 2003, **31(4)**, pp. 417-423

[23] Gatet, L., Tap-Béteille, H., Lescure, M.: Analog Neural Network Implementation for a Real-Time Surface Classification Application', *IEEE Sens J.'*, 2008, **8(7)**, pp. 1413-1421

[24] Zivojinovic, P., Lescure, M., Tap-Béteille, H.: 'Improvement of a CMOS Dual Photosensor for Laser Distance Measurement by a Floating PN Junction', *Sensor Actuat. A-Phys*, 2004, **115**, pp. 273-279

[25] Jackson, J.C. et al.: 'Integrated Bulk/SOI APD sensor: Bulk Substrate Inspection with Geiger-Mode Avalanche Photodiodes', *Electron. Lett.*, 2003, **39(9)**, pp. 735-736

[26] Gatet, L., Tap-Béteille, H., Bony, F.: 'Comparison between Analog and Digital Neural Network Implementations for Range-Finding Applications', *IEEE T. Neural Netw.*, 2009, **20(3)**, pp. 460-470

[27] Baud, C., Tap-Béteille, H., Lescure, M., Béteille, J-P.: 'Analog and Digital Implementation of an Accurate Phasemeter for Laser Range-Finding', *Sensor Actuat. A-Phys*, 2006, **132**, pp. 258-264

[28] Lescure, M., Ganibal, C., Prajoux, R., Briot, M.: 'Compact robotics perception system based on a laser range-finder coupled with silicon micromirrors', *Opt. Eng.*, 2003, **42(2)**, pp. 2653-2658